REVISTA MATÉRIA V.26 N.02
ISSN 1517-7076 artigos e12997, 2021

Study and characterization of carbon xerogels from tannin-formaldehyde system as catalyst support applications

Mariany Ludgero Maia Gomes [1], Gisele Aparecida Amaral-Labat [1], Ana Paula Silva de Oliveira [1], Mauricio Ribeiro Baldan [1], Adriana Maria da Silva [2]

[1] Laboratório associado de sensores e materiais, LABAS/COCTE/INPE, Avenida dos Astronautas, 1758, Jardim da Granja, CEP: 12227-010, São José dos Campos, SP, Brasil.
[2] Laboratório Associado de Combustão e Propulsão, LABCP/INPE, Rodovia Presidente Dutra, km 40, CEP: 12630-970, Cachoeira Paulista, SP, Brasil.
e-mail: mariany.ludgero@inpe.br, silvadeoliveira.ana@gmail.com, gisele.amarallabat@gmail.com, mrbaldan@gmail.com, adriana.silva@inpe.br

ABSTRACT

This contribution reports the use of an organic gel, xerogel, as catalyst support for Cu. The xerogel was synthesized from the system tannin-formaldehyde at pH 3, using F-127 Pluronic as surfactant. The surface area values were higher than 900 m^2/g even after the Cu (10%, wt) impregnation. The morphological analysis by SEM-FEG revealed the presence of spheres arranged in a tridimensional structure. XRD diffractograms showed the presence of CuO and Cu_2O crystalline phases combined with the amorphous structure of the porous carbon. From XRD analysis it is possible to infer the Cu species are heterogeneously dispersed on the support with the co-existence of small and larger clusters, which is in agreement with Raman spectroscopy. Raman study also indicated a highly defect/disorder structure of the xerogel derivatives, ensuing the short-range structural order of the carbonic structure and oxygen groups decorating the carbon surface. XPS results corroborate with XRD and Raman results, detecting the presence of CuO and Cu_2O. In addition to the mentioned Cu species, XPS also detected Cu^0 which may be originated from the chemical interaction between the electron oxygen groups with the Cu precursor. The high surface area and the thermal stability (~ 300 ^oC) of Cu/XCTF envisages its feasibly for relevant catalytic applications.

Keywords: Carbon xerogels, tannin, renewable process, catalyst support.

1. INTRODUCTION

Porous carbon-based structures appeared as a promising material with potential applications in several relevant knowledge fields as catalysis, purification, adsorption, energy storage, to mention few. The literature reports several kinds of porous carbon materials obtained from different raw materials and protocols synthesis [1]. Among them, carbon gels have a different porous structure consisting of a monolithic architecture [2], with a broad range of pores including micro, meso and macropores. The outstanding feature of the porous gels is the possibility of tailoring their physico-chemical properties as pore size distribution and chemical surface by adjusting synthesis conditions [2]. Xerogels can be produced from cheap carbon sources as agriculture waste [3] and inexpensive coal [4, 5], meeting environmental and economical requirements [3, 4]. A potential precursor for carbon gels is the tannin which demonstrated to be efficient to provide a high surface area (up to 900 m^2/g) along with high porosity, 99 % [6-8]. Tannin is natural biopolymer extracted from plants and based on polyphenolic compounds, the condensed flavonoids. These species are reactive with formaldehyde and responsible to the network tridimensional formation of the carbon xerogel [9]. Besides, this biosourced compound is a non-toxic and low-price compared to synthetic phenolics, as resorcinol and phenol, used for the same purpose

Autor Responsável: Mariany Ludgero Maia Gomes Data de envio: 10/03/2020 Data de aceite: 26/03/2021

10.1590/S1517-707620210002.1297

[6, 7, 9].The synthesis of xerogels comprises the polycondensation reaction with subsequent drying under subcritical conditions. The system-resorcinol-formaldehyde is the mostly monomers used for the organic gel synthesis, allowing the design of the desired properties of the final solid. All the steps involved in the xerogel production affect directly the final characteristics of the resulting solid. Nevertheless, the pH of the precursor solution and the concentration of the reactants have a predominant role over the carbon gel properties, where changes in these parameters can lead to a highly porous gel or a completely non-porous carbon [10].

Xerogels have some special properties as high surface area, controllable pores size and chemical surface which make them appropriate to be employed as support for metallic nanoparticles [11]. The high concentration of oxygen-containing groups can act as a nucleation center or anchoring sites for the metallic particles providing an enhanced metallic dispersion and, preventing sintering [11, 12]. The incorporation of oxygen groups (carboxylic anhydrides, lactones, phenol/ether and carbonyl/quinone groups) takes place during the carbonization stage [13].

Thus, the use of xerogel as catalysts support can be a strategy for promoting a high metallic dispersion and stability toward sintering. Moreover, the metal particles recovering by the support burning is another potential advantage related to carbon materials. Therefore, the objective of this research was to design a xerogel from the tannin-formaldehyde system with a high surface area aiming at improving the metallic dispersion of Cu, with a narrow distribution of particle sizes.

2. MATERIALS AND METHODS

2.1. Catalyst synthesis

The organic xerogel was synthesized using tannin as a precursor following the detailed procedure described elsewhere [7], [14]. Briefly, 3 g of the surfactant F-127 Pluronic® (BASF) (~12600 g/mol) was dissolved in 40.84 mL (36 g) of ethanol/water solution (1:1) followed by the gradual addition of tannin powder (6 g). Then, 11 mL (12g) of an aqueous solution of formaldehyde (37%) was poured into the system. After, the pH of the reaction medium was adjusted to 3.0 with concentrated sulfuric acid (98%) in order to avoid dilution issues. The gelation of the material was carried out in a sealed container at 85 °C, for 5 days. In the subsequent step, the material was dried at room temperature for 5 days (subcritical drying). The pyrolysis step of the xerogel was performed in a tubular oven under an argon atmosphere at 900 ºC for 2 h [2, 7]. The pyrolysis temperature was reached using a heating rate of 10 °C/min.

The catalyst was prepared through the incipient wetness impregnation using an aqueous solution of $Cu(NO_3)_2.3H_2O$ (2.14 mol/L). The nominal Cu load was 10%, wt. After impregnation, the sample was dried at 120 ºC, for 12 hours. The samples were thermally treated under the N_2 flow at 300 ºC (heating rate of 5° C/min), for 2 hours.

Samples of carbon xerogel and carbon xerogel impregnated were labeled as XCTF and Cu/XCTF, respectively.

2.2. Catalyst characterization

XRD patterns were recorded on the X-Pert Pro diffractometer from Panalytical using Cu-Kα radiation (Ni filter, $\lambda_{K\alpha 1}$ = 1.5406 Å). The diffraction patterns were obtained at room temperature in the 2θ range from 5° to 70° with step of 0.02°.

Thermal analysis was carried out in a TA analyzer (STA 443 Jupiter/Netzsch) by heating the sample from room temperature to 800 °C (heating rate of 5 °C/min) under air flow (100 mL/min).

The N_2 adsorption measurements were carried out at low temperature of liquid N_2 (-196 °C) on ASAP 2020 Plus instrument, from Micromeritics. Before the adsorption-desorption experiments, the samples were outgassed under vacuum at 200 °C for 48 h.

The morphological study of the samples was carried out using a Scanning Electron Microscopy equipped with a

field emission gun TESCAN, operating at 5.0 kV. The samples were analyzed without metallic coating. All the Energy Dispersive Spectra (EDS) were collected using an EDS system (Oxford Instruments, model X-MaxN 50) integrated to the microscope.

The backscattered Raman spectra were collected using a Horiba Scientific spectrometer (Laboram HR Evolution model) under an excitation laser light wavelength of 514 nm.

XPS analyses were performed with a Kratos Axis Ultra DLD spectrometer equipped with a monochromatic X-ray source of Al Kα (1486.6 eV) at a power of 120 W (operating about at 30μA and 12 kV). All the analysis was realized in a high vacuum analytical chamber maintained below 7 x 10^{-9} torr during spectral acquisition. A charge neutralizer system was used during spectral acquisition. Prior to measurements, the samples were outgassing in the sample treatment chamber (STC) before insertion into the sample analysis chamber (SAC). The survey spectrum was obtained in the binding energy range from 0 to 1200 eV at pass energy of 160 eV. High-resolution scans of the O1s, C1s, and Cu2p regions were collected at pass energy of 40 eV. The XPS data were analyzed through CasaXPS software (version 2.3.16). A standard Shirley background subtraction was used for binding energy quantitative analysis. All XPS spectra were deconvoluted with Gaussian Lorentzian mixed function. Atomic concentration was calculated using peak areas from the survey spectra.

3. RESULTS AND DISCUSSION

The materials phase compositions were assessed by X-Ray Diffraction (Figure 1). The diffraction pattern acquired for the XCTF support exhibited peaks at 2θ = 25.3° and 2θ = 44.3°, characteristics of the basal planes of graphite [15], with a striking broadening resulting from the disordered carbon phase. It is worth to notice that even after the carbonization treatment at 900 °C, the character amorphous of the xerogel structure was kept. This behavior is interesting since, during the carbonization process, most of the volatile compounds and moisture are removed which could result in shrinkage leading to a modification in the porous structure. The diffraction pattern obtained for the Cu/XCTF catalyst exhibited, in addition to the amorphous carbon phase, diffraction lines corresponding to copper oxides. The peaks at 2θ = 36.56° and 42.39° are attributed to the planes (111) and (200) of the cubic phase of Cu_2O [16], respectively. The peak at 2θ = 29.78° corresponding to the plane (110) of Cu_2O can not be clearly identified due to the peak overlapping with the carbon plane.

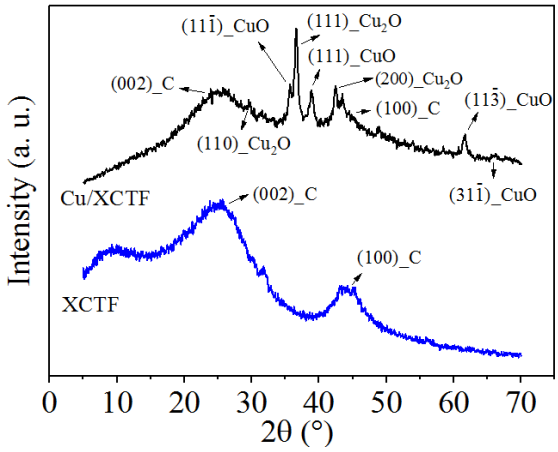

Figure 1: Diffraction patterns for XCTF and Cu/XCTF.

The peaks at 2θ = 35.5°, 38.7°, 61.5° and 66,2° are associated to the planes (11-1), (111), (11-3) and (31-1) of CuO [17]. The shape of all the peaks related to Cu species indicates higher structural order than carbon support, presenting a slightly higher intensity. Furthermore, it is noticeable a broadening at the base of these peaks, suggesting a heterogeneous crystallite sizes, with the co-existence of small and large Cu aggregates.

The thermal stability of catalysts has a critical role since catalytic reactions are performed under high temperature and distinct atmosphere as H_2, CO_2, O_2, etc. Thus, the thermal stability of the Cu/XCTF sample under air flow was inves-

tigated by TGA analysis, as depicted in Figure 2. The loss weight profile presents two thermal events one at 67 °C, corresponding to the elimination of physisorbed H_2O. The second thermal comprises a broad range of temperature, beginning at 270 °C and finishing around 500 °C, with a shoulder at 289 °C. The shoulder can be attributed to the decomposition of unstable groups decorating the xerogel surface as hydroxyl, epoxy, carbonyl and carboxyl groups [18]. The second stage of of the peak can be associated to the carbon lattice burning, as evidenced by similar carbon structures, whose mass spectra of the TGA effluent revealed only the presence of H_2O and CO_2 [12]. The remaining mass detected in weigh loss profile is around of 6 % and can be ascribed to Cu oxides. The thermal stability of the Cu/XCTF system make it a potential candidate for many relevant catalytic reactions, including the CO_2 hydrogenation.

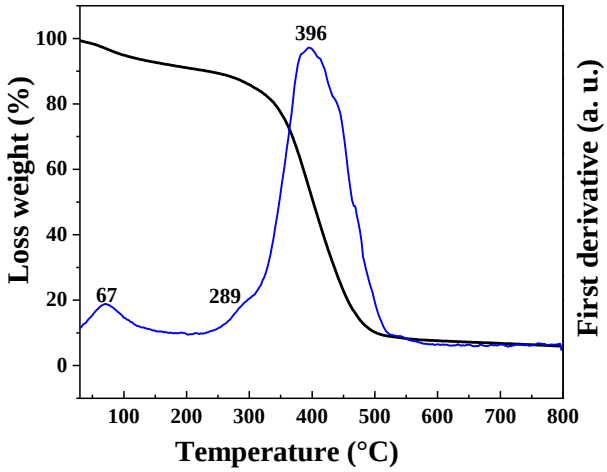

Figure 2: TGA, Loss weight and first derivative of the loss weight profiles of Cu/XCTF.

The N_2 isotherms adsorption/desorption of both samples were type I (Figure 3), according to the IUPAC classification, showing a large microporosity related. Furthermore, the hysteresis indicates the presence of mesoporosity due to the capillary condensation phenomenon [19]. The textural parameters of those samples were calculated and are shown in Table 1. All the samples showed elevated micropore volumes and slightly mesoporosity developed (Table 1). The XCTF presented a higher surface area value than the catalyst support, probably due to the presence of Cu on the carbon, which may lead to a pore blockage by the deposition of metallic particles. Nonetheless, the catalyst support still presented a developed surface area, suitable for catalytic reactions applications. The remarkable result presented here is the high surface area value (> than 900 m^2/g) for the supported catalyst, which is crucial for the stabilization of Cu species at the nanoscale level.

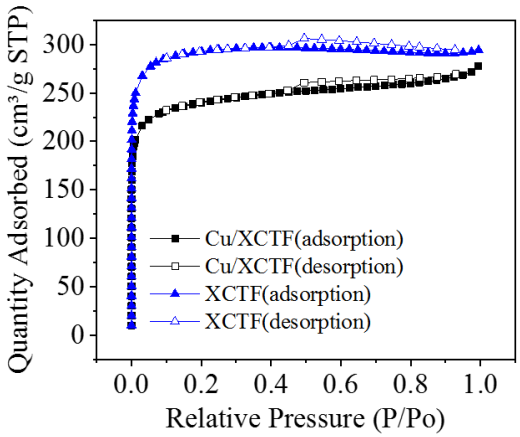

Figure 3: Nitrogen adsorption–desorption isotherms at 77 K (full and open symbols, respectively) of both samples.

Table 1: Textural parameters of samples: BET surface area (S_{BET}), total pore volume at p/p0 = 0.99 ($V_{total\ 0.99}$), micropore (V_{DR}) and mesopore (V_{meso}) volumes, and micropore and mesopore fractions. t-plot values are also presented: micropore volume (V_u), and micropores (S_{micro}) and external (S_{ext}) surface areas.

			Dubinin method (DR)				t-plot		
Sample	S_{BET} ($m^2\ g^{-1}$)	$V_{total\ 0.99}$ ($cm^3\ g^{-1}$)	V_{DR} ($cm^3\ g^{-1}$)	V_{meso} ($cm^3\ g^{-1}$)	V_{DR} / $V_{0.99}$	V_{meso} / $V_{0.99}$	V_u ($cm^3\ g^{-1}$)	S_{micro} ($m^2\ g^{-1}$)	S_{ext} ($m^2\ g^{-1}$)
XCTF	1158	0.45	0.44	0.01	0.99	0.01	0.40	1026	132
Cu/XCTF	934	0.43	0.39	0.04	0.91	0.09	0.29	756	178

The pore size distribution, calculated from DFT (Density Functional Theory) method, is given in Figure 4. The original sample XCTF was essentially microporous, showing pores smaller than 1 nm. After the impregnation and calcination, the sample presented micropores between 1 nm and 1.4 nm and mesoporosity in the range from 5 to 18 nm and, thus, present-ing a bimodal pores distribution. Although the main contribution for the high surface area stems from the high microporosi-ty, the bimodal pores distribution is important for catalysis applications. The pores size in catalytic reactions is connected with molecule accessibility to the active sites inside the pores. The internal part of the micropores will be accessible only for small molecules, whereas it will be blocked for higher compounds. Taking account that catalytic phenomena are driven by mass transport, intra-particle diffusion limitation can take place mainly in micropores [20]. Thus, the development of catalysts with bimodal pore sizes distribu-tion is crucial to ensure the mass transport inside the pores for higher molecules.

The pore sizes is related to the sites accessibility and mass transport diffusion.

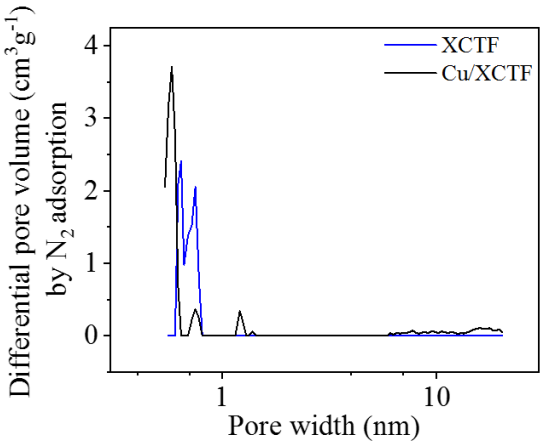

Figure 4: The pore size distribution, calculated from DFT (Density Functional Theory) method.

The morphological analysis of the samples XCTF and Cu/XCTF were evaluated by Scanning Electron Microscopy (SEM/FEG), Figure 5. The sample XCTF images exhibited spherical nodules arranged in a tridimensional structure, typical of carbon xerogels from tannin-formaldehyde [9]. The size of the nodules is related to the tannin concentration and especially to the initial pH in the reaction medium [9]. All these factors control the final properties of the XCTF after the carbonization process. With regarding the catalyst Cu/XCTF, the spherical nodules are still present though their distribution is more heterogeneous. In addition, a white texture can be observed on the surface matrix, suggesting a Cu deposition over the morphological structure.

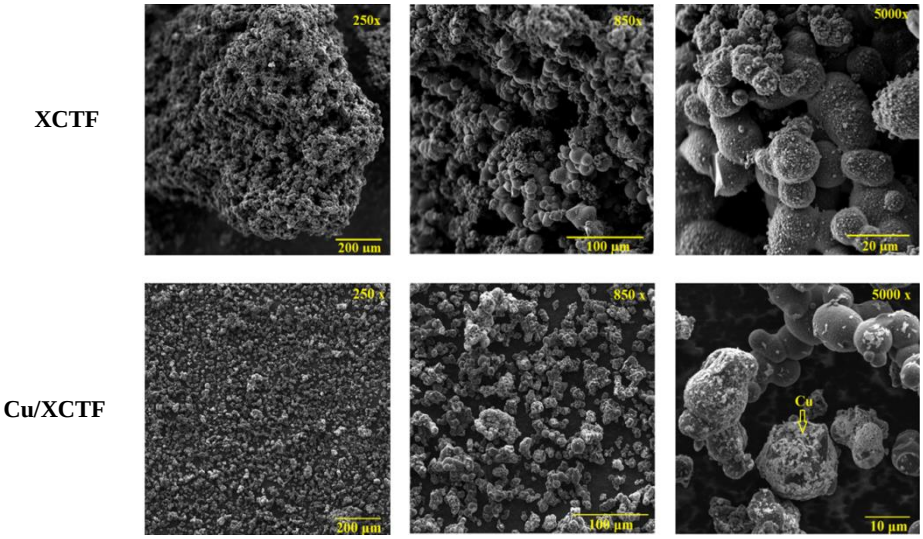

Figure 5: SEM-FEG images of XCTF and Cu/XCTF samples, at 250x, 850x and 5000x magnifications.

EDS mapping was performed to show the distribution of Cu structures on the surface of the carbonaceous material (XCTF). The Cu element distribution is shown in Figure 6. Table 2 compiles the semiquantitative results of the EDS analysis. Although EDS is a punctual analysis and may not reflect all the heterogeneous catalyst surface, the amount of Cu is within an acceptable level with relation the nominal content of Cu (10 %, wt).

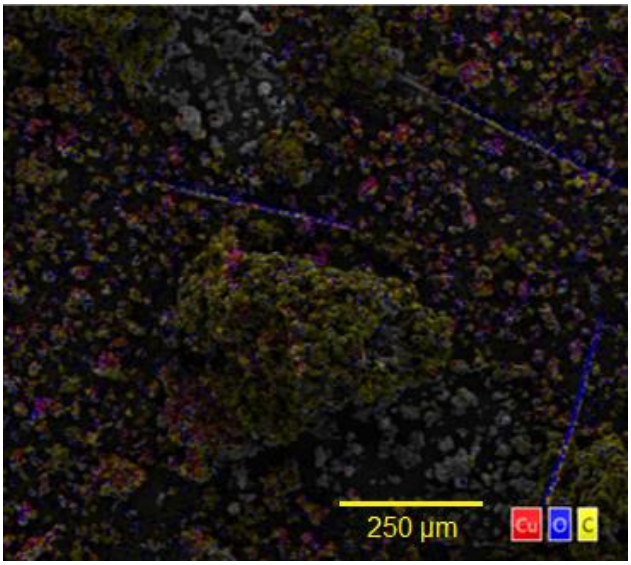

Figure 6: EDS mapping of Cu/XCTF sample.

Table 2: EDS data for the Cu/XCTF sample.

Sample	Composition (wt.%)		
	Cu	O	C
Cu/XCTF	13.6	18.1	68.3

The samples were also investigated by Raman Spectroscopy with the purpose of evaluating their structural integrity (Figure 7). Both spectra exhibited features characteristics of carbon structure as the defect-induced D band and first-order Raman active G band at 1350 cm^{-1} and 1600 cm^{-1}, respectively. The presence of the D-band and its blue shift in comparison with the band in the defects absence (1580 cm^{-1}) denotes a rich defective structure, resulting from the short-range

structural order of the porous carbon structure and surface oxygen. The catalyst Cu/XCTF spectrum also exhibited bands attributed to CuO (294, 345 and 633 cm^{-1}). The appearance of such features in the spectrum is a strong indicative of some CuO aggregates deposited on the catalyst support [21]. Indeed, XRD pattern evidences the co-existence of small and large particles in the catalyst.

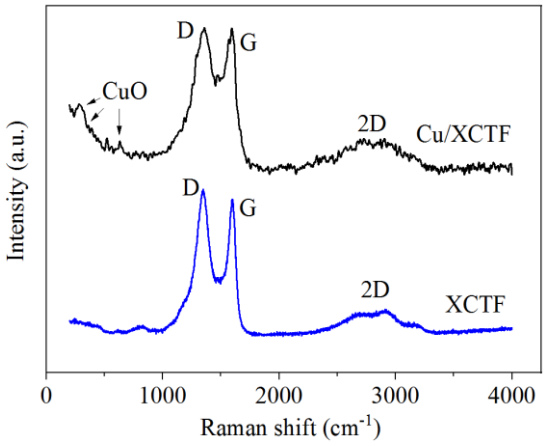

Figura 7: Raman spectra of the samples XCTF (A) and Cu/XCTF (B).

The XPS survey spectrum, Figure 8, exhibited two peaks, related to the elements, C(1s) and O(1s) at binding energy 286.4 eV and 531 eV respectively, for the sample XCTF (A). The same can be observed for the sample Cu/XCTF (B), however, for the latter, there are observed also peaks from the Cu 2p element, at binding energy 950 eV. For both samples, the analyses were carried out with prolonged exposure time.

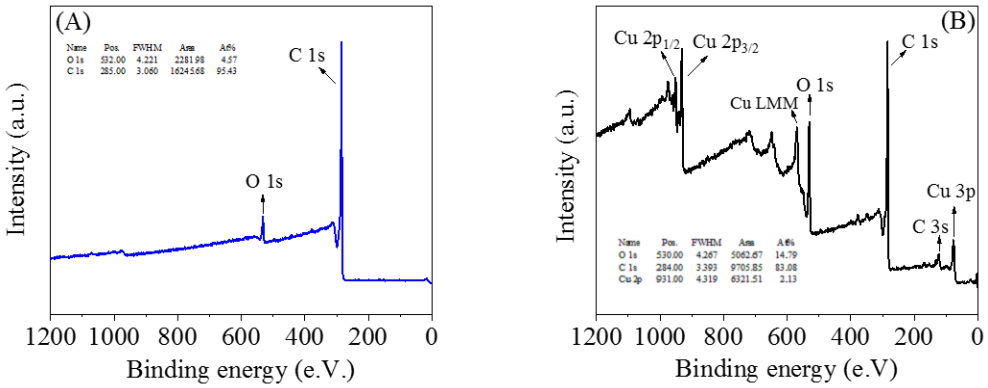

Figure 8: XPS Survey spectrum for the sample XCTF (A), and for the same sample after the impregnation process with Cu, Cu/XCTF (B).

Figure 9 presents a high-resolution XPS spectrum of Cu 2p to obtain more insight into the chemical composition of Cu/XCTF. The presence of two majors peak, at binding energy 934.54 eV and 954.39 eV, are associated with the typical Cu $2p_{3/2}$ and Cu $2p_{1/2}$. The relative intensities of the doublet peaks for p subshells are equal to ½. The factor two relative to the difference between intensities comes from the ratio of their respective degeneracies [22]. The binding energy separation between the peaks is 19.85 eV, indicating the presence of oxidation states of Cu, and in good agreement with the values reported in the literature. Besides, the existence of a strong satellite peak, which is caused by electron shake-up process, at 943.97 eV indicates that Cu predominantly exists as Cu^{2+} [23]. It is important to notice that existence of satellite peaks is characteristic of CuO [22]. This result may be corroborated by Raman active modes at 294, 345 and 633 cm^{-1}, which is identified as the first order phonon scattering [24]. The fitted Cu $2p_{3/2}$ is relatively complex with different components corresponding to various chemical states. The presence of a shoulder at 933.04 eV may be associated to Cu metal

and the other two peak profile at 934.64 and 936.51 eV are relatively broad, which may suggest the presence of other Cu species.

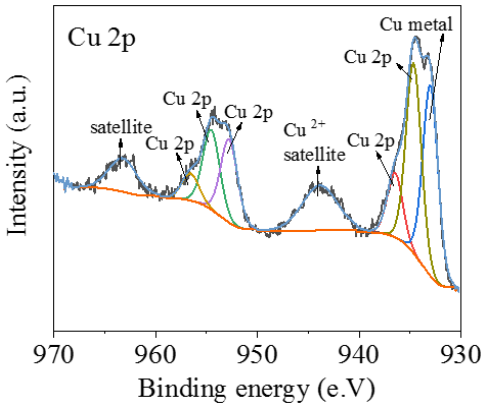

Figure 9: XPS High-resolution spectrum of Cu(2p).

It worth pointing out that the presence of the reduced Cu in the catalysts, which can be associate to a chemical interaction with the electron oxygen groups present in the xerogel surface. In addition to Cu^0, copper oxide was also present suggesting different interactions degree between oxygen surface groups and metal.

4. CONCLUSION

The synthesis of xerogel from tannin is a promising route in order to provide a carbon gel with high surface area. The high surface area combined with the good thermal stability envisages the xerogel as potential support for catalytic applications. Moreover, different Cu species were distributed on the support indicating distinct interaction between Cu precursor salt and oxygen functionalities. Indeed, Raman spectroscopy of the samples under investigation was rich defective structures due to the presence of oxygen groups attached to the xerogel surface.

The presence of such chemical groups is beneficial under the catalysis perspective, which may become the solid surface unstable, facilitating the interaction reactant catalyst. XRD and Raman gave indications of a heterogeneous Cu particles sizes distribution on the support. Additional studies are already being conducted with the purpose of optimizing the physical-chemical properties of the support and consequently increase the distribution and, stabilizing the Cu particles.

5. ACKNOWLEDGEMENTS

This study was financed in part by the Coordenação de Aperfeiçoamento de Pessoal de Nível Superior – Brasil (CAPES) – Finance Code 001, and FAPESP (2018/18798-2).

6. BIBLIOGRAPHY

[1] LEE, J., KIM, J., HYEON, T. "Recent progress in the synthesis of porous carbon materials," doi: 10.1002/adma.200501576. *Adv. Mater.*, v. 18, n. 16, pp. 2073-2094, 2006.
[2] GRISHECHKO, L.I., AMARAL-LABAT, G., FIERRO, V., *et al.*, "Biosourced, highly porous, carbon xerogel microspheres," doi: 10.1039/c6ra09462g. *RSC Adv.*, v. 6, n. 70, pp. 65698-65708, 2016.
[3] SEYEDSADR, S., AL AFIF, R., PFEIFER, C. "Hydrothermal carbonization of agricultural residues: A case study of the farm residues -based biogas plants," doi: 10.1016/j.crcon.2018.06.001, *Carbon Resour. Convers.*, v. 1, n. 1, pp. 81-85, 2018.
[4] SHARMA, A., SAKIMOTO, N., TAKANOHASHI, T. "Effect of binder amount on the development of coal-binder interface and its relationship with the strength of the carbonized coal-binder composite," doi: 10.1016/j.crcon.2018.05.002, *Carbon Resour. Convers.*, v. 1, n. 2, pp. 139-146, 2018.
[5] ALWADANI, N., FATEHI, P. "Synthetic and lignin-based surfactants: Challenges and opportunities," doi: 10.1016/j.crcon.2018.07.006, *Carbon Resour. Convers.*, v. 1, n. 2, pp. 126-138, 2018.
[6] SZCZUREK, A., AMARAL-LABAT, G., FIERRO, V., *et al.*, "The use of tannin to prepare carbon gels. Part I: Carbon aerogels," doi: 10.1016/j.carbon.2011.03.007. *Carbon N. Y.*, v. 49, n. 8, pp. 2773-2784, 2011,

[7] AMARAL-LABAT, G., SZCZUREK, A., FIERRO, V., *et al.*, "Unique bimodal carbon xerogels from soft templating of tannin," doi: 10.1016/j.matchemphys.2014.10.006. *Mater. Chem. Phys.*, v. 149, pp. 193-201, 2015.
[8] AMARAL-LABAT, G., *et al.*, "Pore structure and electrochemical performances of tannin-based carbon cryogels," doi: 10.1016/j.biombioe.2012.01.019, *Biomass and Bioenergy*, v. 39, pp. 274-282, 2012,
[9] BRAGHIROLI, F.L., AMARAL-LABAT, G., BOSS, A.F.N., *et al.*, "Tannin gels and their carbon derivatives: A review," doi: 10.3390/biom9100587. *Biomolecules*, v. 9, n. 10, 2019.
[10] ANGEL, E.G.J., ARENILLAS, A. "Designing Nanostructured Carbon Xerogels," in *Nanomaterials*, 2011.
[11] MALDONADO-HÓDAR, F.J., PÉREZ-CADENAS, A.F., MORENO-CASTILLA, C. "Morphology of heat-treated tunsgten doped monolithic carbon aerogels," doi: 10.1016/S0008-6223(03)00069-1. *Carbon N. Y.*, v. 41, n. 6, pp. 1291-1299, 2003.
[12] FRANCHINI, C.A., LLORCA, J., KUZNETSOV, A., *et al.*, "Outstanding dispersion of CeO2 on reduced graphene oxide. Implications for highly dispersed Pd catalysts," doi: 10.1016/j.diamond.2020.108061, *Diam. Relat. Mater.*, v. 109, n. August, 2020.
[13] FIGUEIREDO, J.L., PEREIRA, M.F.R., SERP, P., *et al.*, "Development of carbon nanotube and carbon xerogel supported catalysts for the electro-oxidation of methanol in fuel cells," doi: 10.1016/j.carbon.2006.05.033. *Carbon N. Y.*, v. 44, n. 12, pp. 2516-2522, 2006.
[14] AMARAL-LABAT, G., GRISHECHKO, L.I., FIERRO, V., *et al.*, "Tannin-based xerogels with distinctive porous structures," doi: 10.1016/j.biombioe.2013.06.001. *Biomass and Bioenergy*, v. 56, pp. 437-445, 2013.
[15] YUE, X., ARENILLAS, A., IRVINE, J.T.S. "Application of infiltrated LSCM-GDC oxide anode in direct carbon/coal fuel cells," doi: 10.1039/c6fd00001k , *Faraday Discuss.*, v. 190, pp. 269-289, 2016.
[16] XIONG, L., *et al.*, "Fast and simplified synthesis of cuprous oxide nanoparticles: Annealing studies and photocatalytic activity," doi: 10.1039/c4ra12406e . *RSC Adv.*, v. 4, n. 107, pp. 62115-62122, 2014.
[17] LI, Z., XIN, Y., ZHANG, Z., *et al.*, "Rational design of binder-free noble metal/metal oxide arrays with nanocauliflower structure for wide linear range nonenzymatic glucose detection," doi: 10.1038/srep10617. *Sci. Rep.*, v. 5, pp. 1-10, Jan. 2015.
[18] MOUSSA, S., SIAMAKI, A.R., GUPTON, B.F., *et al.*, "Pd-partially reduced graphene oxide catalysts (Pd/PRGO): Laser synthesis of pd nanoparticles supported on PRGO nanosheets for carboncarbon cross coupling reactions," doi: 10.1021/cs200497e . *ACS Catal.*, v. 2, n. 1, pp. 145-154, 2012.
[19] KENNETH STAFFORD WILLIAM SING, "INTERNATIONAL UNION OF PURE COMMISSION ON COLLOID AND SURFACE CHEMISTRY INCLUDING CATALYSIS * REPORTING PHYSISORPTION DATA FOR GAS / SOLID SYSTEMS with Special Reference to the Determination of Surface Area and Porosity," *Area*, v. 57, n. 4, pp. 603-619, 1985.
[20] SÁNCHEZ-POLO, M., LEYVA-RAMOS, R., RIVERA-UTRILLA, J. "Kinetics of 1,3,6-naphthalenetrisulphonic acid ozonation in presence of activated carbon," doi: 10.1016/j.carbon.2004.11.027. *Carbon N. Y.*, v. 43, n. 5, pp. 962-969, 2005.
[21] LI, H., *et al.*, "Regulation of Cu species in CuO/SiO2 and its structural evolution in ethynylation reaction," doi: 10.3390/nano9060842. *Nanomaterials*, v. 9, n. 6, 2019.
[22] PAULY, N., TOUGAARD, S., YUBERO, F. "Determination of the Cu 2p primary excitation spectra for Cu, Cu 2O and CuO," doi: 10.1016/j.susc.2013.10.009. *Surf. Sci.*, v. 620, pp. 17-22, 2014.
[23] DIN, I.U., *et al.*, "Carbon nanofibers based copper /zirconia catalysts for carbon dioxide hydro- genation to methanol: Effect of copper concentration," 2017.
[24] AKGUL, F.A., AKGUL, G., YILDIRIM, N., *et al.*, "Influence of thermal annealing on microstructural, morphological, optical properties and surface electronic structure of copper oxide thin films," doi: 10.1016/j.matchemphys.2014.06.047. *Mater. Chem. Phys.*, v. 147, n. 3, pp. 987-995, 2014.

ORCID

Mariany Ludgero Maia Gomes https://orcid.org/0000-0002-2645-4145
Gisele Aparecida Amaral-Labat https://orcid.org/0000-0003-3745-6119
Ana Paula Silva de Oliveira https://orcid.org/0000-0002-9701-3566
Maurício Ribeiro Baldan https://orcid.org/0000-0002-4465-3834
Adriana Maria Da Silva https://orcid.org/0000-0002-5022-2758